This is the accepted manuscript of Riihelä, A., Bright, R. M., & Anttila, K. (2021).
Recent strengthening of snow and ice albedo feedback driven by Antarctic sea-ice loss. Nature Geoscience, 14(11), 832–836.
The version of record can be accessed at https://doi.org/10.1038/s41561-021-00841-x

Recent strengthening of snow and ice albedo feedback driven by Antarctic sea ice loss

Aku Riihelä[1], Ryan M. Bright[2], and Kati Anttila[1]

Affiliations

[1]*Finnish Meteorological Institute, FI-00560, Helsinki, Finland*

[2]*Norwegian Institute of Bioeconomy Research, Box 115, 1431 Ås, Norway*

Corresponding author: Aku Riihelä, aku.riihela@fmi.fi

The decline of the Arctic cryosphere during recent decades has lowered the region's surface albedo, reducing its ability to reflect solar radiation back to space. It is not clear what role the Antarctic cryosphere plays in this regard, but novel remote-sensing based techniques and datasets have recently opened the possibility to investigate its role. Here, we leverage these to show that the surface albedo reductions from sustained post-2000 losses in Arctic snow and ice cover equate to increasingly positive snow and ice albedo feedback relative to a 1982-1991 baseline period, with a decadal trend of +0.08 ± 0.04 W/m^2/dec. between 1992-2015. During the same period, the expansion of the Antarctic sea ice pack generated a negative feedback, with a decadal trend of -0.06 ± 0.02 W/m^2/dec. However, significant Antarctic sea ice losses during 2016 - 2018 completely reversed the trend, increasing the three-year mean combined Arctic and Antarctic snow and ice albedo

feedback to +0.26 ± 0.15 W/m^2. This reversal highlights the importance of Antarctic sea ice loss to the global snow and ice albedo feedback. The 1992-2018 mean feedback is equivalent to approximately 10% of anthropogenic CO2 emissions over the same period; the share may rise markedly should 2016-2018 snow and ice conditions become common, though increasing longwave emissions will likely mediate the impact on the total radiative energy budget.

Changes in the properties and extent of the Polar Regions' snow and ice cover alter the surface reflectivity or albedo, leading to a change in the shortwave radiative energy balance at the edge of Earth's atmosphere, known as snow and ice albedo feedback (SIAF). The magnitude of this radiative feedback for a particular surface albedo change is primarily determined by available insolation and atmospheric properties which affect radiative transfer, such as cloudiness [1 - 3]. These relationships are variable in space and time and are generally quantified in radiative feedback calculations as variables called radiative kernels. These kernels have typically been derived from climate models [4], leading to omission of temporal (interannual) variability and to close ties between the radiative transfer processes in a specific climate model and the associated radiative feedback per unit surface albedo change. Recent progress in satellite remote sensing techniques has allowed for observation-based derivation of radiative kernels, which, unlike model-derived kernels, enable the capturing of interannual trends in important atmospheric state variables affecting radiative transfer. This makes them well-suited to quantify radiative feedbacks in regions like the Arctic that experience high interannual variability in cloud area fraction and aerosol optical depth [5] -- two important atmospheric state properties affecting shortwave radiative transfer. Combined with multidecadal satellite-based surface albedo time series which allow for robust trend assessments [6] it is now possible to comprehensively assess SIAF caused by ongoing changes in the snow and ice cover of Earth's Polar regions.

This is the accepted manuscript of Riihelä, A., Bright, R. M., & Anttila, K. (2021).
Recent strengthening of snow and ice albedo feedback driven by Antarctic sea-ice loss. Nature Geoscience, 14(11), 832–836.
The version of record can be accessed at https://doi.org/10.1038/s41561-021-00841-x

Here, we focus on quantifying the evolution of both Arctic and Antarctic (defined as all regions poleward of ±50 degrees latitude) SIAF based on aforementioned radiative kernels and surface albedo changes between 1982 and 2018, relative to a baseline period of 1982-1991. There are two distinct advantages to this approach. First, the effect of bias in surface albedo estimates is eliminated because we deal with differential albedo, and second, we avoid having to prescribe the cryospheric extent and albedo characteristics of the reference period, as those are drawn from the early period of the observed data itself.

We use a satellite observation-based surface albedo data record with over three and a half decades of global coverage from the AVHRR optical imager family [7]. The dataset has been shown to produce consistent surface albedo trends with other satellite-based datasets over the Arctic [6,8,9]. We employ two state-of-the-art observation-based radiative kernels; the CALIPSO-CloudSat (henceforth CC) kernel derived from active lidar/radar observations of the atmosphere, clouds, and underlying surface [10], and the CERES Albedo Change Kernel (CACK) [11], which is based on multiyear observations of shortwave radiative fluxes in the Earth's atmosphere-surface system by the CERES sensor [12]. The availability of the CC and CACK kernels represents a major advance in the field, as they allow for more fully observation-driven radiative feedback estimates independent of climate models' radiative transfer processes or atmospheric composition.

Arctic and Antarctic snow and ice albedo feedback

Figure 1 shows the global annual mean SIAF summed over the two regions (Figure 1a), as well as the Arctic and Antarctic components separately (Figure 1b & 1c). The combined annual mean SIAF averages +0.08 W/m^2 for the period outside the baseline (1992-2018), but we also observe a rapid rise to +0.26 W/m^2 for the 2016-2018 mean. To place the result in context, the 1992-2018 mean SIAF is equivalent to an annual pulse emission of ~3.8 Gt of CO_2 [13], representing approximately 10% of global anthropogenic CO_2 emissions over the same period. Should 2016-2018 conditions persist, the fraction would increase towards 30%.

Over the Arctic, the increasing trend in SIAF (+0.08 ± 0.03 W/m^2/decade for 1992-2018) is consistent with a wide range of literature documenting e.g. the retreat of the Arctic Ocean's ice cover [e.g. 14], or the trend towards spring snow cover reduction and earlier melt onset of the hemisphere's seasonal snow cover [15, 16]. The annual SIAF in 2008, 0.19 ± 0.1 W/m^2 with CC and 0.15 ± 0.08 W/m^2 with CACK kernels over the global area (i.e. 0.37 ± 0.19 and 0.29 ± 0.17 W/m^2 regionally), is consistent with earlier published estimates which analyzed reductions in cryospheric radiative cooling between 1979 and 2008, yielding a central range of 0.38 – 0.59 W/m^2 for the Arctic area [2]. The generally increasing trend in Arctic SIAF was interrupted by the relatively cool and cloudy summer of 2013 which inhibited surface melt across many parts of the Arctic cryosphere [17] and thus kept the region's surface albedo closer to baseline period conditions.

In contrast, Antarctic SIAF was generally negative and decreasing from the turn of the millennium until 2014 (Figure 1c). This decrease in SIAF is consistent with well documented, although only partially understood, expansion of the Antarctic sea ice pack [18]. However, in 2016-2018 Antarctic SIAF showed a dramatic increase, which completely reversed the 15-year trend towards decreasing RF relative to the baseline period. This reversal is particularly significant because during the 2000-2015 period the combined Arctic and Antarctic SIAF (Figure 1a) had been close to balanced (mean of +0.06 W/m^2), with albedo increases from Antarctic sea ice expansion offsetting albedo decreases from the retreat of Arctic sea ice and snow cover. With the Antarctic cryosphere's SIAF turning from net negative to positive, we see the aforementioned rapid rise in combined cryospheric SIAF in 2016-2018 to a level which triples the overall 1992-2018 mean.

This is the accepted manuscript of Riihelä, A., Bright, R. M., & Anttila, K. (2021).
Recent strengthening of snow and ice albedo feedback driven by Antarctic sea-ice loss. Nature Geoscience, 14(11), 832–836.
The version of record can be accessed at https://doi.org/10.1038/s41561-021-00841-x

Antarctic snow and ice albedo feedback reversal

To better understand the causes of the reversal in the Antarctic SIAF trend, we delineated both Arctic and Antarctic SIAF into oceanic and terrestrial domains, as shown in Figure 2. The steady increases in Arctic terrestrial and oceanic SIAF are clear, with the sea ice-related oceanic SIAF being somewhat larger as also reported by earlier studies [2, 19]. Furthermore, the delineation shows that the cause of the Antarctic SIAF increase since 2016 is almost solely attributable to sea ice changes. This is again fully consistent with independent, microwave-based satellite observations which showed a sudden loss of the Antarctic sea ice, beginning in 2016 and persisting through 2018 [18].

To further assess the consistency between the Antarctic SIAF increase and reported sea ice losses, we examine the spatial distribution of the feedback during the consecutive three-year periods of 2013-2015 and 2016-2018 (Figure 3; also see Fig. S11). The patterns reveal clear shifts from negative to positive SIAF, particularly over the Weddell and Ross Seas, but also over a part of the Western Pacific Ocean. In comparison, the Indian Ocean sector saw relatively limited changes. This spatial pattern is very consistent with the distribution of the sea ice coverage reductions as seen by microwave satellite instruments, particularly occurring during the Austral spring of 2016 [18, 20]. Recent studies on the principal causes of the sudden and dramatic shift in Antarctic sea ice point to an array of oceanic and atmospheric drivers acting partly consecutively and partly in concert, but affecting various Antarctic Seas differently [21, 22].

For a longer-term verification, we compared our oceanic annual mean SIAF against microwave satellite observation-based annual mean estimates for Arctic and Antarctic Sea Ice Extent (SIE; [23]) and Sea Ice Concentration (SIC; [24]). Robust agreement was found between SIAF and SIC over both regions, (Fig. S4), and between SIAF and SIE over the Arctic (Fig. S5). A stronger correlation against SIC is expected, as sea ice concentration changes reflect albedo changes better than sea ice extent. While SIC estimates contain large uncertainties during the melting season, the biases are ameliorated in large-scale aggregates as used here [25]. Furthermore, the feedback incurred from the post-millennium Arctic sea ice losses is in good agreement with recent independent estimates, which estimated +0.11 W/m^2 for the period 2000-2016 from CERES satellite observations [26], while our estimates yield +0.08 W/m^2 for the CACK and +0.13 W/m^2 for the CC kernel (details in Supplementary Material).

While the escalating feedback impact from mounting Arctic snow and sea ice losses remains clear, the magnitude of the combined Arctic and Antarctic SIAF since 2016 also clearly illustrates the scope of the recent Antarctic sea ice changes, and underlines the need to better understand whether the ice loss is indicative of a systemic state shift or an expression of large-scale variability in the Antarctic cryosphere.

Drivers of recent Antarctic sea ice changes

The causes of the sudden reversal in the Antarctic sea ice pack's expansion is an area of active research. A common reported theme is that the atmospheric circulation over Antarctic seas in and since 2016 has been anomalous. A key feature has been the formation of several abnormally intense and long-lasting low pressure systems (cyclones) during austral spring and summer, which act to both compress the sea ice pack against Antarctica at the eastern flank of the cyclone, and to increase sea ice drift to lower latitudes (where melt will more easily claim it) along the western flank [20, 27, 28]. Associated advection of warm and moist air masses from lower latitudes have also been indicated as a contributor to melt increase, alongside a sustained buildup of anomalously warm upper ocean temperatures over the Southern Ocean [17]. Also, the removal of sea ice via drifting in early spring can trigger an amplification of the sea ice loss via the sea ice albedo feedback [29].

The question of whether or not this reversal represents natural variability or a state shift remains open. Latest research indicates a partial recovery of the sea ice in 2020 [30], and proxy-based reconstructions of Antarctic sea ice extent suggest large natural variability during the past 200 years [31]. However, our ability to model and predict the evolution of the sea ice pack is hampered by continued underestimation of Antarctic sea ice coverage and large inter-model spread even in the most state-of-the-art climate models [32]. A recent study proposed that the handling of thermodynamic ocean-atmosphere coupling over the Southern Ocean is a key source of these discrepancies [33]. Given the demonstrated importance of Antarctic sea ice to the global SIAF, further attention to this topic is certainly warranted.

Cryospheric albedo and radiative flux trends in CERES EBAF

To gauge the relevance of SIAF in relation to other radiative feedbacks of the global cryosphere (both shortwave (SW) and longwave (LW)), we analyzed a 20-yr. CERES EBAF v4.1 time series [12] of TOA radiative fluxes and surface albedo over both the Arctic and Antarctic regions (see Supplementary Figures S7-S10 for details). Figure 4 (left panel) shows that – collectively – the net SW budget (SW_{net}) over the cryosphere is strongly and significantly correlated ($r = 0.9$) to the surface albedo, suggesting that the upward trend in SW_{net} (Fig. 4, right panel, red) is likely attributed to the albedo change-driven feedback. The annual variability and trend in CERES-based SW_{net} is similar (Pearson's $r = 0.78$) to the post-2000 upward trend in SW SIAF derived from radiative kernels and CLARA-A2 (Fig. 1a), although the SW_{net} trend is stronger (+0.017 W/m^2/yr for SW_{net} vs. +0.01 W/m^2/yr for SIAF in Jan-Dec 2001-2018). The difference likely consists principally of cloudiness change impacts on TOA SW_{net}, although the cool Arctic summer of 2013 also exerts a notable influence on the SIAF trend (which is +0.012 W/m^2/yr with 2013 excluded). Also, significant annual variability infers a large uncertainty envelope of ±0.01 W/m^2/yr to the SIAF trend.

Our analysis also reveals that SIAF is likely the dominant feedback mechanism behind the upward trend seen in the net radiative balance of the cryosphere (Fig. 4, right panel, blue). An enhanced outgoing LW emission over the same period, however, has dampened the albedo-change driven SW_{net} change by about 45%, inferred by comparing slopes of the two trend lines shown in Fig. 4 (right), although the mechanism is unclear. The significant linear upward trends in the cryospheric radiative budget appear to be the result of opposing anomalies occurring near-simultaneously in the Arctic and Antarctic regions, which is particularly pronounced during the 2016-2018 period (Figs. S7 & S8). In the Antarctic, SW_{net} and Net radiative fluxes and trends over the past 10 years are intimately coupled and significant in the months Nov., Dec., Jan., and Mar. and appear to dominate the annual regional energy balance (Fig. S9). As expected, seasonal Antarctic surface albedo and SW_{net} are strongly correlated during austral spring and summer (Fig. S10).

Estimating the surface albedo feedback parameter

Combining our multidecadal radiative feedback estimates with global near-surface air temperature data allows us, in principle, to estimate the cryospheric surface albedo feedback parameter (λ_α) which quantifies the sensitivity of albedo feedback to global warming. Regressing our two-kernel mean Arctic SIAF against 1992-2018 global annual mean air temperatures from the MERRA-2 [34] and ERA5 [35] atmospheric reanalyses, we obtained sensitivities of +0.39 $W/m^2/K$ and +0.24 $W/m^2/K$, respectively. While markedly different, the estimates agree with a recently published estimate of +0.27 ± 0.18 $W/m^2/K$ [35] within the uncertainty bounds.

However, for the Antarctic, we find that cooling associated with the sea ice expansion until 2016 dominates the regression, leading to a negative best-fit feedback parameter (details in Supplementary Material, pg. 8). The result echoes a recent study [32] on the portrayal of Antarctic

This is the accepted manuscript of Riihelä, A., Bright, R. M., & Anttila, K. (2021).
Recent strengthening of snow and ice albedo feedback driven by Antarctic sea-ice loss. Nature Geoscience, 14(11), 832–836.
The version of record can be accessed at https://doi.org/10.1038/s41561-021-00841-x

sea ice area in observations versus climate models. The root cause for the discrepancy may be that the response of the Antarctic cryosphere to increased warming occurs at time scales longer than our available datasets, despite their decadal coverage [37].

Uncertainty considerations

We consider our SH SIAF estimate to be robust given the harmony between the CACK- and CC-based estimates (Fig 1b). The bulk of the disagreement in NH SIAF between CACK- and CC-based estimates can likely be explained by discrepancies in prescribed atmospheric states underlying the two kernels in the region, and specifically, to differences in cloud fraction and the cloud detection methods behind these. Cloud fraction in CERES EBAF-TOA v4 (underlying CACK) is based on a passive optical detection algorithm [12, 38], whereas cloud detection in the CloudSat/CALIPSO algorithm (underlying CC) is based on a combination of active lidar and radar [39]. We infer through statistical analysis that discrepancies in prescribed NH (50° - 80° N) cloud fraction indeed may explain a large portion of the disagreement between the two kernels (Fig. S1), where signs of kernel differences largely align with that of differences in underlying cloud fractions, which is particularly prominent for the months of May - October (Fig. S2).

Remaining discrepancies between the two kernels may be attributed to differences in other prescribed atmospheric state variables affecting shortwave radiative transfer (e.g., scattering aerosols, cloud phase and optical depth) or to differences in the radiative transfer calculations themselves. The effect of the time-dependent atmospheric background state underlying CACK compared to the fixed atmosphere of CC provides little explanation for the discrepancy in our NH RF estimates (Fig. S3).

The role of aerosols in explaining observed trends in the surface SW radiative energy budget was studied by first estimating their direct impact on the surface albedo. Over polar cryospheres, the aerosol optical depth (AOD) is typically <0.1 [40]. There have been observations of AOD change over the recent years by 0.2 [3]. The possible effect of AOD changing by 0.2 on surface albedo has been estimated to be 0.06 at extreme cases [16]. For most of the cases the effect was much less. The change in surface albedo due to melt of sea ice is in the range of 0.6, thus giving a ten times larger effect on albedo than the change in aerosols.

To assess whether the recently observed AOD anomalies in the Antarctic [3] might explain observed trends in the TOA SW radiation budget over the region, we filtered out the fraction of outgoing SW radiation at TOA attributable to the surface albedo (using the model of [41]) and found no appreciable residual trend that could be attributable to the remaining bulk radiative constituents such as aerosols, ozone, and water vapor. If aerosols are playing a role, it is being obfuscated by counteracting trends in one or more of the other constituents (Fig. S6).

All of the Antarctic SIAF is of cryospheric origin, but because we calculate SIAF for all areas poleward of 50° N/S, a fraction of the Arctic feedback originates from non-cryospheric land surface albedo changes. However, during the SIAF growth period from 2004 onwards, the contribution from non-cryospheric regions has been less than 20% of the total annual mean. This confirms that also the lion’s share of the observed Arctic SIAF is a result of cryospheric changes, i.e. losses and gains in snow and sea ice cover.

Acknowledgments

Work of A.R. has been financially supported by the Academy of Finland, decision 309125, and R.M.B through the Research Council of Norway, project number 294948 (EMERALD). Natural Earth map dataset is acknowledged as the coastline data source in spatially resolved figures.

Author Contributions

A.R. designed the study and performed the SIAF calculations. R.M.B. contributed CACK data with updated uncertainty estimates, analyzed CACK-CC differences, and carried out the CERES EBAF analysis. K.A. supported the SIAF analysis and analyzed potential aerosol impacts. A.R., R.M.B. and K.A. all contributed to the writing of the manuscript.

Competing Interests

The authors declare no competing interests.

Figure Captions

Figure 1: The annual global mean snow/ice albedo feedback (SIAF) [W/m2] resulting from white-sky surface albedo changes for a) both Arctic and Antarctic cryospheres as the two-kernel mean, as well as b) Arctic and c) Antarctic regions separately. Red and blue colors indicate SIAF calculated with the CloudSat-CALIPSO (CC) and CERES Albedo Change Kernel (CACK) kernels (respectively). Shaded areas indicate uncertainty envelopes. All values are calculated against a baseline period of 1982-1991.

Figure 2: Three-year global annual mean snow/ice albedo feedback (SIAF) induced primarily by cryospheric albedo changes for a) Arctic, and b) Antarctic. Blue bars indicate oceanic and orange bars terrestrial SIAF. Red lines indicate the summed SIAF for the Arctic and Antarctic. Calculated with the CACK kernel.

Figure 3: Three-year mean snow/ice albedo feedback (SIAF) with the CACK kernel over the Antarctic during a) 2013-2015, and b) 2016-2018, relative to the baseline period of 1982-1991. Color bar truncated to better highlight smaller SIAF.

Figure 4. Cryosphere contribution to global mean net shortwave energy balance (SW_{net}) plotted as a function of the cryosphere contribution to global mean surface albedo (left); cryosphere contribution to global mean SW_{net} and net radiative balance (SW_{net} - LW↑, TOA) of the past 20 years (1 March 2000 – 29 February 2020; right). Signs are positive downward. Refer to Eq. (1) for a definition of the cryosphere contribution to global means. For reference, global annual mean SW_{net} and Net radiative fluxes for the first (last) year of the series are 240.7 (242.3) and 0.87 (1.41) W m-2, respectively. Calculated slopes are in W/m2/yr.

References

1. Sledd, A., & L'Ecuyer, T. (2019). How much do clouds mask the impacts of Arctic sea ice and snow cover variations? Different perspectives from observations and reanalyses. *Atmosphere*, *10*(1), 12.
2. Flanner, M. G., Shell, K. M., Barlage, M., Perovich, D. K., & Tschudi, M. A. (2011). Radiative forcing and albedo feedback from the Northern Hemisphere cryosphere between 1979 and 2008. *Nature Geoscience*, *4*(3), 151-155.
3. Loeb, N., Thorsen, T., Norris, J., Wang, H., & Su, W. (2018). Changes in Earth's Energy Budget during and after the "Pause" in Global Warming: An Observational Perspective. Climate, 6(3), 62. https://doi.org/10.3390/cli6030062
4. Chung, E.-S., and Soden, B. J.: An assessment of methods for computing radiative forcing in climate models, Environmental Research Letters, 10, 074004, 10.1088/1748-9326/10/7/074004, 2015.
5. Dong, X., Xi, B., Crosby, K., Long, C. N., Stone, R. S., & Shupe, M. D. (2010). A 10 year climatology of Arctic cloud fraction and radiative forcing at Barrow, Alaska. *Journal of Geophysical Research: Atmospheres*, *115*(D17).
6. Zhang, R., Wang, H., Fu, Q., Rasch, P. J., & Wang, X. (2019). Unraveling driving forces explaining significant reduction in satellite-inferred Arctic surface albedo since the 1980s. *Proceedings of the National Academy of Sciences*, *116*(48), 23947-23953.
7. Karlsson, K. G., Anttila, K., Trentmann, J., Stengel, M., Meirink, J. F., Devasthale, A., ... & Benas, N. (2017). CLARA-A2: the second edition of the CM SAF cloud and radiation data record from 34 years of global AVHRR data. *Atmospheric Chemistry and Physics*, *17*(9), 5809-5828.
8. Anttila, K., Jääskeläinen, E., Riihelä, A., Manninen, T., & Andersson, K. (2016). Algorithm theoretical basis document: CM SAF Cloud, Albedo, Radiation Data Record,

AVHRR-Based, Edition 2 (CLARA-A2)—surface albedo. EUMETSAT Satellite Application Facility on Climate Monitoring Doc. SAF/CM/FMI/ATBD/GAC/SAL, 85 pp., https://www.cmsaf.eu

9. Riihelä, A., King, M. D., & Anttila, K. (2019). The surface albedo of the Greenland Ice Sheet between 1982 and 2015 from the CLARA-A2 dataset and its relationship to the ice sheet's surface mass balance. The Cryosphere, 13(10), 2597-2614.
10. Kramer, R. J., Matus, A. V., Soden, B. J., & L'Ecuyer, T. S. (2019). Observation-based radiative kernels from CloudSat/CALIPSO. *Journal of Geophysical Research: Atmospheres*, *124*(10), 5431-5444.
11. Bright, R. M. and O'Halloran, T. L. (2019). Developing a monthly radiative kernel for surface albedo change from satellite climatologies of Earth's shortwave radiation budget: CACK v1.0, Geosci. Model Dev., 12, 3975–3990, https://doi.org/10.5194/gmd-12-3975-2019, 2019.
12. Loeb, N. G., Doelling, D. R., Wang, H., Su, W., Nguyen, C., Corbett, J. G., ... & Kato, S. (2018). Clouds and the earth’s radiant energy system (CERES) energy balanced and filled (EBAF) top-of-atmosphere (TOA) edition-4.0 data product. *Journal of Climate*, *31*(2), 895-918.
13. Betts, R. A. (2000). Offset of the potential carbon sink from boreal forestation by decreases in surface albedo. Nature, 408(6809), 187-190.
14. Kwok, R. (2018). Arctic sea ice thickness, volume, and multiyear ice coverage: losses and coupled variability (1958–2018). *Environmental Research Letters*, *13*(10), 105005.
15. Wang, L., Derksen, C., Brown, R., & Markus, T. (2013). Recent changes in pan-Arctic melt onset from satellite passive microwave measurements. Geophysical Research Letters, 40(3), 522-528.
16. Anttila, K., Manninen, T., Jääskeläinen, E., Riihelä, A., & Lahtinen, P. (2018). The role of climate and land use in the changes in surface albedo prior to snow melt and the timing

of melt season of seasonal snow in northern land areas of 40 N–80 N during 1982–2015. Remote Sensing, 10(10), 1619.

17. Jeffries, M. O., J. A. Richter-Menge, and J. E. Overland, Eds., 2013: Arctic Report Card 2013, http://www.arctic.noaa.gov/reportcard.
18. Parkinson, C. L. (2019). A 40-y record reveals gradual Antarctic sea ice increases followed by decreases at rates far exceeding the rates seen in the Arctic. *Proceedings of the National Academy of Sciences*, 116(29), 14414-14423.
19. Letterly, A., Key, J., & Liu, Y. (2018). Arctic climate: Changes in sea ice extent outweigh changes in snow cover*. The Cryosphere*, 12(10), 3373-3382.
20. Turner, J., Phillips, T., Marshall, G. J., Hosking, J. S., Pope, J. O., Bracegirdle, T. J., & Deb, P. (2017). Unprecedented springtime retreat of Antarctic sea ice in 2016. *Geophysical Research Letters*, 44(13), 6868-6875.
21. Wang, G., Hendon, H.H., Arblaster, J.M. et al. (2019). Compounding tropical and stratospheric forcing of the record low Antarctic sea-ice in 2016. *Nat Commun* 10, 13. https://doi.org/10.1038/s41467-018-07689-7
22. Meehl, G.A., Arblaster, J.M., Chung, C.T.Y. et al. (2019). Sustained ocean changes contributed to sudden Antarctic sea ice retreat in late 2016. *Nat Commun* 10, 14. https://doi.org/10.1038/s41467-018-07865-9
23. Fetterer, F., K. Knowles, W. N. Meier, M. Savoie, and A. K. Windnagel. (2017), updated daily. Sea Ice Index, Version 3. [Northern and Southern Hemispheres]. Boulder, Colorado USA. NSIDC: National Snow and Ice Data Center. doi: https://doi.org/10.7265/N5K072F8. [Date Accessed: Oct 1, 2010]
24. Meier, W. N., F. Fetterer, M. Savoie, S. Mallory, R. Duerr, and J. Stroeve. (2017). NOAA/NSIDC Climate Data Record of Passive Microwave Sea Ice Concentration, Version 3. [Northern and Southern Hemispheres]. Boulder, Colorado USA. NSIDC:

National Snow and Ice Data Center. doi: https://doi.org/10.7265/N59P2ZTG. [Date Accessed: Oct 1, 2010].

25. Kern, S., Lavergne, T., Notz, D., Pedersen, L. T., and Tonboe, R. (2020). Satellite passive microwave sea-ice concentration data set inter-comparison for Arctic summer conditions, *The Cryosphere*, 14, 2469–2493, https://doi.org/10.5194/tc-14-2469-2020
26. Pistone, K., Eisenman, I., & Ramanathan, V. (2019). Radiative Heating of an Ice-Free Arctic Ocean. *Geophysical Research Letters*, 46(13), 7474-7480.
27. Schlosser, E., Haumann, F. A., and Raphael, M. N. (2018). Atmospheric influences on the anomalous 2016 Antarctic sea ice decay, *The Cryosphere*, 12, 1103–1119, https://doi.org/10.5194/tc-12-1103-2018
28. Wang, Z., J. Turner, Y. Wu, and C. Liu, (2019). Rapid Decline of Total Antarctic Sea Ice Extent during 2014–16 Controlled by Wind-Driven Sea Ice Drift. *J. Climate*, 32, 5381–5395, https://doi.org/10.1175/JCLI-D-18-0635.1.
29. Kashiwase, H., Ohshima, K. I., Nihashi, S., & Eicken, H. (2017). Evidence for ice-ocean albedo feedback in the Arctic Ocean shifting to a seasonal ice zone. *Scientific Reports*, 7(1), 1-10.
30. Eayrs, C., Li, X., Raphael, M. N., & Holland, D. M. (2021). Rapid decline in Antarctic sea ice in recent years hints at future change. Nature Geoscience, 14(7), 460-464.
31. Jones, J., Gille, S., Goosse, H. et al. (2016). Assessing recent trends in high-latitude Southern Hemisphere surface climate. *Nature Clim Change* 6, 917–926. https://doi.org/10.1038/nclimate3103
32. Roach, L. A., Dörr, J., Holmes, C. R., Massonnet, F., Blockley, E. W., Notz, D., ... & Bitz, C. M. (2020). Antarctic sea ice area in CMIP6. *Geophysical Research Letters*, 47(9), e2019GL086729.

33. Chemke, R., & Polvani, L. M. (2020). Using multiple large ensembles to elucidate the discrepancy between the 1979–2019 modeled and observed Antarctic sea ice trends. *Geophysical Research Letters*, 47(15), e2020GL088339.

34. Gelaro, R., McCarty, W., Suárez, M. J., Todling, R., Molod, A., Takacs, L., ... & Zhao, B. (2017). The modern-era retrospective analysis for research and applications, version 2 (MERRA-2). Journal of climate, 30(14), 5419-5454.

35. Hersbach, H., Bell, B., Berrisford, P., Hirahara, S., Horányi, A., Muñoz-Sabater, J., ... & Thépaut, J. N. (2020). The ERA5 global reanalysis. Quarterly Journal of the Royal Meteorological Society, 146(730), 1999-2049.

36. Donohoe, A., Blanchard-Wrigglesworth, E., Schweiger, A., & Rasch, P. J. (2020). The Effect of Atmospheric Transmissivity on Model and Observational Estimates of the Sea Ice Albedo Feedback. Journal of Climate, 33(13), 5743-5765.

37. Hall, A. (2004). The role of surface albedo feedback in climate. Journal of Climate, 17(7), 1550-1568.

38. Platnick, S., King, M. D., Ackerman, S. A., Menzel, W. P., Baum, B. A., Riédi, J. C., & Frey, R. A. (2003). The MODIS cloud products: Algorithms and examples from Terra. *IEEE Transactions on Geoscience and Remote Sensing*, 41(2), 459-473.

39. Kay, J. E., & Gettelman, A. (2009). Cloud influence on and response to seasonal Arctic sea ice loss. *Journal of Geophysical Research: Atmospheres*, 114(D18).

40. Tomasi, C., Lupi, A., Mazzola, M., Stone, R. S., Dutton, E. G., Herber, A., ... & Vitale, V. (2012). An update on polar aerosol optical properties using POLAR-AOD and other measurements performed during the International Polar Year. Atmospheric Environment, 52, 29-47.

41. Donohoe, A., & Battisti, D. S. (2011). Atmospheric and surface contributions to planetary albedo. Journal of Climate, 24(16), 4402-4418.

This is the accepted manuscript of Riihelä, A., Bright, R. M., & Anttila, K. (2021).
Recent strengthening of snow and ice albedo feedback driven by Antarctic sea-ice loss. Nature Geoscience, 14(11), 832–836.
The version of record can be accessed at https://doi.org/10.1038/s41561-021-00841-x

Methods

Snow/ice albedo feedback calculation

The global snow/ice albedo feedback is calculated as follows:

$$SIAF = \frac{1}{A}\sum_n k_n * (\alpha_n - \alpha_n^{BL}) * A_n \quad (1)$$

Where A_n represents the grid cell area, k_n represents the all-sky radiative kernel, and α_n^{BL} and α_n indicate the baseline and observed white-sky surface albedos valid for the location and time of each grid cell *n.* We calculate SIAF separately for the Arctic and Antarctic at the monthly scale for all areas poleward of 50 degrees latitude, gap-filling as necessary (see below). To obtain global annual means, we sum SIAF over the study regions for each month, average over a full year, then normalize to Earth's total surface area (A). We also calculate uncertainty envelopes for SIAF, based on a conservative assessment of uncertainty arising from gaps in the albedo record as well as uncertainties in the albedo estimates and kernels (see below for details). Where shown, trend magnitudes and uncertainties are calculated with outlier-resistant Theil-Sen linear regressions with 95% confidence intervals.

Albedo data processing

Our albedo estimates are based on the CLARA-A2.1 SAL dataset [7], which offers global surface albedo estimates at 0.25 degree / 25 km spatial resolution as 5-day and monthly means. The record spans 01/1982 - 06/2019, here we use the full annual coverage period of 1982-2018. We emphasize that the surface albedo record provides extensive coverage of the Arctic and Antarctic melting seasons where the vast majority of the SIAF originates. The albedo retrievals used in this

This is the accepted manuscript of Riihelä, A., Bright, R. M., & Anttila, K. (2021).
Recent strengthening of snow and ice albedo feedback driven by Antarctic sea-ice loss. Nature Geoscience, 14(11), 832–836.
The version of record can be accessed at https://doi.org/10.1038/s41561-021-00841-x

study are constructed from intercalibrated satellite data from instruments onboard different satellites.

The CLARA-A2.1 black-sky surface albedo products are based on intercalibrated [42] satellite observations from the AVHRR instruments onboard the NOAA and MetOP satellites. The intercalibration ensures a temporally stable data record with a possibility to study decadal trends. The stability of the intercalibrated CLARA-A2 albedo record was assessed and found to be ~8% (relative) over the central parts of the Greenland Ice Sheet.

The top-of-atmosphere reflectances observed by the satellites go through various steps while being processed into Earth surface albedo: First the cloudy observations are removed and the underlying surface classified (snow & ice, land, water), using microwave observations to verify the classification over sea ice. Then for the land areas the atmospheric effect on the observed reflectance is taken into account using dynamic aerosol optical depth description [43] and the topographic effects of the surface on the location and reflectance are corrected over mountainous terrain. To derive the hemispherical reflectance from the bidirectional satellite observation, the surface scattering properties are described by using bidirectional reflectance distribution functions (BRDF) for different land use types. For snow/ice covered surfaces there are no globally valid scattering models. Therefore, the albedo for these surfaces is treated as the average of observations from different viewing directions during the month in question, relying on comprehensive angular sampling from wide-swath AVHRR observations. The observations of 0.6 and 0.8 μm are then converted to describe the albedo at 0.25 - 2.5 μm wavelengths, the algorithm adjusting for wet and dry snow/ice surfaces.

To obtain bihemispherical (white-sky) albedo estimates for this study, we convert the CLARA-A2.1 black-sky albedos with empirically based equations [44]. The equations are separate for snow/ice, vegetation, and snowy forests; NSIDC0046 [45] snow/sea ice cover and ESA-CCI LC

This is the accepted manuscript of Riihelä, A., Bright, R. M., & Anttila, K. (2021).
Recent strengthening of snow and ice albedo feedback driven by Antarctic sea-ice loss. Nature Geoscience, 14(11), 832–836.
The version of record can be accessed at https://doi.org/10.1038/s41561-021-00841-x

data were used to classify each grid cell of the Arctic region accordingly. Over the Antarctic, snow/ice cover is assumed for all non-open ocean grid cells. G02202 sea ice data [24] is used to identify Antarctic sea ice coverage per month. All data were projected into the 25 km EASE2 projection for analysis, using nearest-neighbor resampling when necessary. White-sky albedo for open water was derived following a recent parameterization [46] using wind speed data as applied in CLARA-A2.1 SAL, but the feedback from open ocean regions was found negligibly small for both Arctic and Antarctic.

The CLARA-A2 SAL data record has been validated against in situ data and compared to the MCD43C3 ed 5 dataset [47]. Based on the comparison with in situ observations, the relative accuracy of the product over snow/ice covered surfaces has been found to be 5-10%. The global coverage including the polar regions, the high quality of the intercalibration of data from different satellites and the long temporal coverage makes this data record particularly useful for climatic studies of the Arctic and Antarctic cryosphere.

CERES EBAF fluxes and surface albedo

The CERES EBAF edition 4.1 dataset covering 2000-2020 [12] was obtained for independent verification of our results. All-sky top-of-atmosphere and surface shortwave and longwave fluxes were extracted for analysis for both polar cryospheres poleward of 50 degrees latitude. EBAF-based surface albedo estimates were derived from the reflected and incoming shortwave fluxes at surface. Further details on CERES EBAF calculations are available in Supplementary Material (pg.11-15).

Gap-filling and uncertainty

To perform the SIAF calculations for the surface albedo coverage period of 1982-2018, the radiative kernels must be available for each examined month. The CC kernel is spatially resolved for each month based on observations from 2008-2009, while the CACK kernel is spatiotemporally resolved for all months between 2001 and 2016. It has been shown that the interannual variability in the radiative kernels is modest compared to spatial and monthly variability, thus ensuring that the CC kernel can be reliably used to represent atmospheric conditions during the post-2000 period [10]. Since the surface albedo changes are defined against a baseline period of 1982-1991, the calculated interannual mean SIAF during 1982-1991 must also be negligible by design. Given these arguments, we backfill both CC and CACK kernels backwards to 1982, and forward to 2018. For CACK we use the 2001-2016 climatology as fill values.

Gaps occur in the albedo data record over areas with persistent cloud cover or insufficient illumination for a reliable retrieval (e.g. polar winter). In the CC kernel, latitudes poleward of 80° have no coverage because of the orbital characteristics of the CALIPSO and CloudSat satellites. We calculated that typically less than 10% of the Arctic or Antarctic SIAF originated from latitudes 80° - 90° N/S between 2000-2018, as both the innermost sea ice zone of the Arctic Ocean and the inner parts of Antarctica have thus far maintained relatively stable snow and ice cover relative to the more outlying regions of the polar cryospheres. We therefore simply gap-filled the CC kernel with the mean kernel value of latitudes 75° - 80° N/S for each studied month. Gaps in the albedo record occur primarily during winter, we therefore gap-filled SIAF over missing albedo data with a period-appropriate, literature-based constant of +0.05 W/m^2 [2]. Choosing to gap-fill with a neutral RF of 0 W/m^2 had no appreciable impact on our global annual mean results.

The uncertainty envelopes in our derived annual mean SIAF were determined as follows. We first calculated a conservative estimate for SIAF that could potentially be missed through gaps in the albedo record, using CC and CACK kernels and prescribed (α-α_{BL}) appropriate for each month (larger values for melting seasons than winter, see Supplementary Material pg. 7-8 for details). Next, we derived uncertainty related to successful SIAF computations, based on a combination of published uncertainties for the kernels and a calculation of uncertainty for the albedo, founded on the number of successful nominal resolution retrievals per grid cell, again with conservative outer bounds (see Supplementary Material pg. 7-8 for details). The larger of these factors on the annual, region-aggregated scale was chosen as the displayed uncertainty for each studied year. We emphasize that the uncertainty envelopes are very conservative in nature and that the largest uncertainties are not likely to be realized. In general, the uncertainty related to the kernels and albedo for successful SIAF calculations is the larger of the two; only in 1984, 1994, and 2000 over the Antarctic the missing data uncertainty was larger because of large data gaps in the albedo record, related to shifts in the AVHRR constellation [7]. For the combined cryospheric annual mean SIAF, the root sum of squared CC and CACK uncertainties is shown in Figure 1.

Data Availability

The principal result data (annual global radiative forcings per kernel and region) are available from
http://doi.org/10.23728/fmi-b2share.fb5a74c32c0b4e49989334f76b370de2
The CLARA-A2.1 albedo data is available from
https://doi.org/10.5676/EUM_SAF_CM/CLARA_AVHRR/V002_01.
The CC radiative kernel is available from https://climate.rsmas.miami.edu/data/radiative-kernels/index.html.
The CACK radiative kernel is available from
https://doi.org/10.6073/pasta/d77b84b11be99ed4d5376d77fe0043d8.
NSIDC0046 and G02202 snow/sea ice data records are available through https://nsidc.org/data.
ESA-CCI LC data is available from the ESA Climate Change Initiative through
http://maps.elie.ucl.ac.be/CCI/viewer/download.php.

The CERES EBAF Edition 4.1 dataset is available through https://asdc.larc.nasa.gov/project/CERES/CERES_EBAF_Edition4.1

Code availability

Principal data analysis codes are available from

http://doi.org/10.23728/fmi-b2share.fb5a74c32c0b4e49989334f76b370de2

Corresponding Author

Correspondence to Aku Riihelä.

References

42. Heidinger, A.K., Straka, W.C., Molling, C.C., Sullivan, J.T., Wu, X.Q. (2010). Deriving an inter-sensor consistent calibration for the AVHRR solar reflectance data record. *International Journal of Remote Sensing*, 31(24), 6493-6517.
43. Jääskeläinen, E., Manninen, T., Tamminen, J., & Laine, M. (2017). The Aerosol Index and Land Cover Class Based Atmospheric Correction Aerosol Optical Depth Time Series 1982–2014 for the SMAC Algorithm. *Remote Sensing*, 9(11), 1095.
44. Manninen, T., Jääskeläinen, E., & Riihelä, A. (2019). Black and White-Sky Albedo Values of Snow: In Situ Relationships for AVHRR-Based Estimation Using CLARA-A2 SAL. *Canadian Journal of Remote Sensing*, 45(3-4), 350-367.
45. Brodzik, M. J. and R. Armstrong. 2013. Northern Hemisphere EASE-Grid 2.0 Weekly Snow Cover and Sea Ice Extent, Version 4. [Arctic coverage]. Boulder, Colorado USA. NASA National Snow and Ice Data Center Distributed Active Archive Center. doi: https://doi.org/10.5067/P7O0HGJLYUQU. [Date Accessed: 1.8.2020].
46. Séférian, R., Baek, S., Boucher, O., Dufresne, J. L., Decharme, B., Saint-Martin, D., & Roehrig, R. (2018). An interactive ocean surface albedo scheme (OSAv1. 0): formulation

and evaluation in ARPEGE-Climat (V6. 1) and LMDZ (V5A). *Geoscientific Model Development*, 11(1), 321-338.

47. Schaaf, C. B., Gao, F., Strahler, A. H., Lucht, W., Li, X., Tsang, T., ... & Lewis, P. (2002). First operational BRDF, albedo nadir reflectance products from MODIS. *Remote sensing of Environment*, 83(1-2), 135-148.

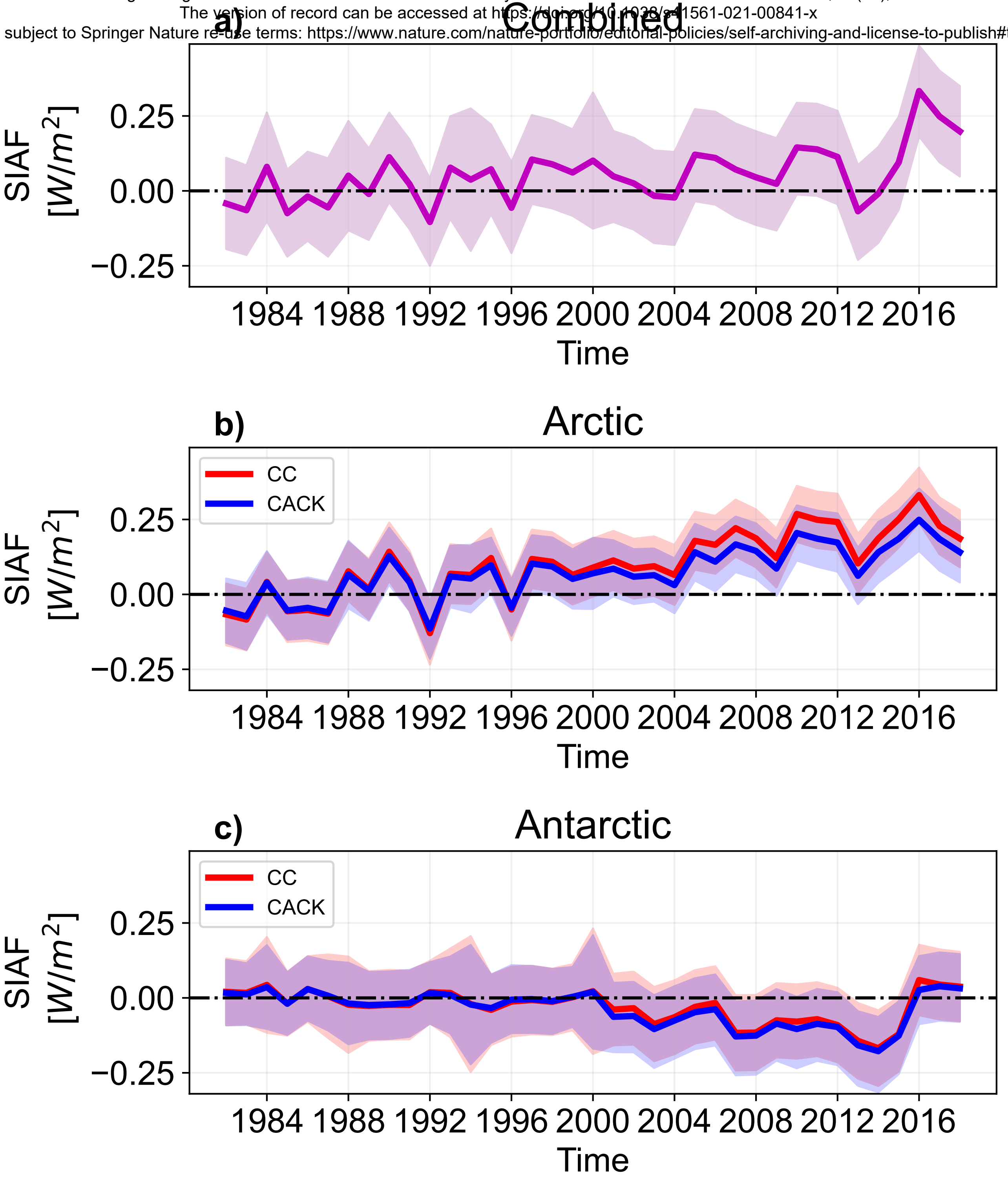
a)
Combined
SIAF [W/m^2]
0.25
0.00
−0.25
1984 1988 1992 1996 2000 2004 2008 2012 2016
Time
b)
Arctic
CC
CACK
SIAF [W/m^2]
0.25
0.00
−0.25
1984 1988 1992 1996 2000 2004 2008 2012 2016
Time
c)
Antarctic
CC
CACK
SIAF [W/m^2]
0.25
0.00
−0.25
1984 1988 1992 1996 2000 2004 2008 2012 2016
Time

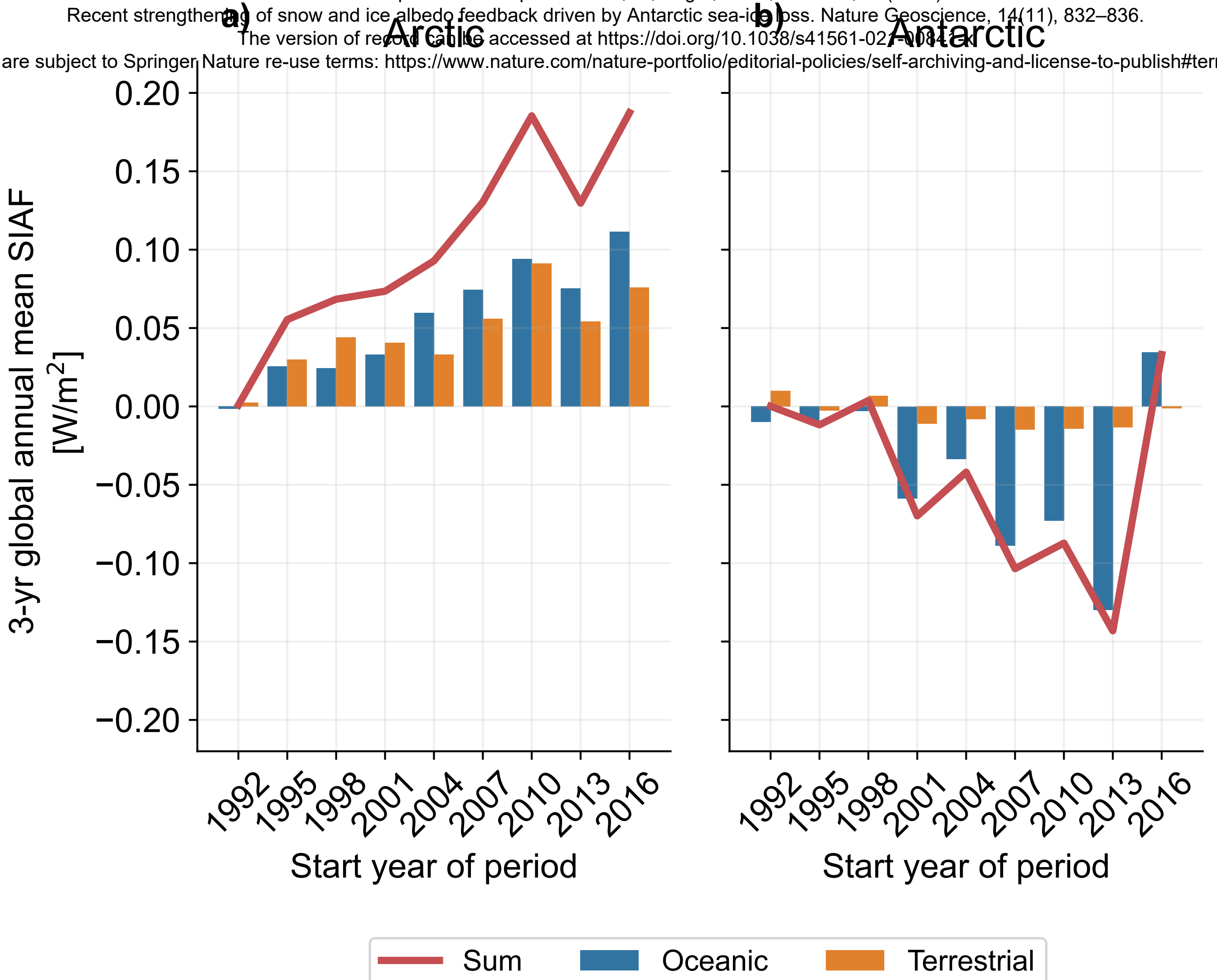
a)
Arctic
b)
Antarctic
3-yr global annual mean SIAF [W/m2]
0.20
0.15
0.10
0.05
0.00
−0.05
−0.10
−0.15
−0.20
1992
1995
1998
2001
2004
2007
2010
2013
2016
Start year of period
Start year of period
Sum
Oceanic
Terrestrial

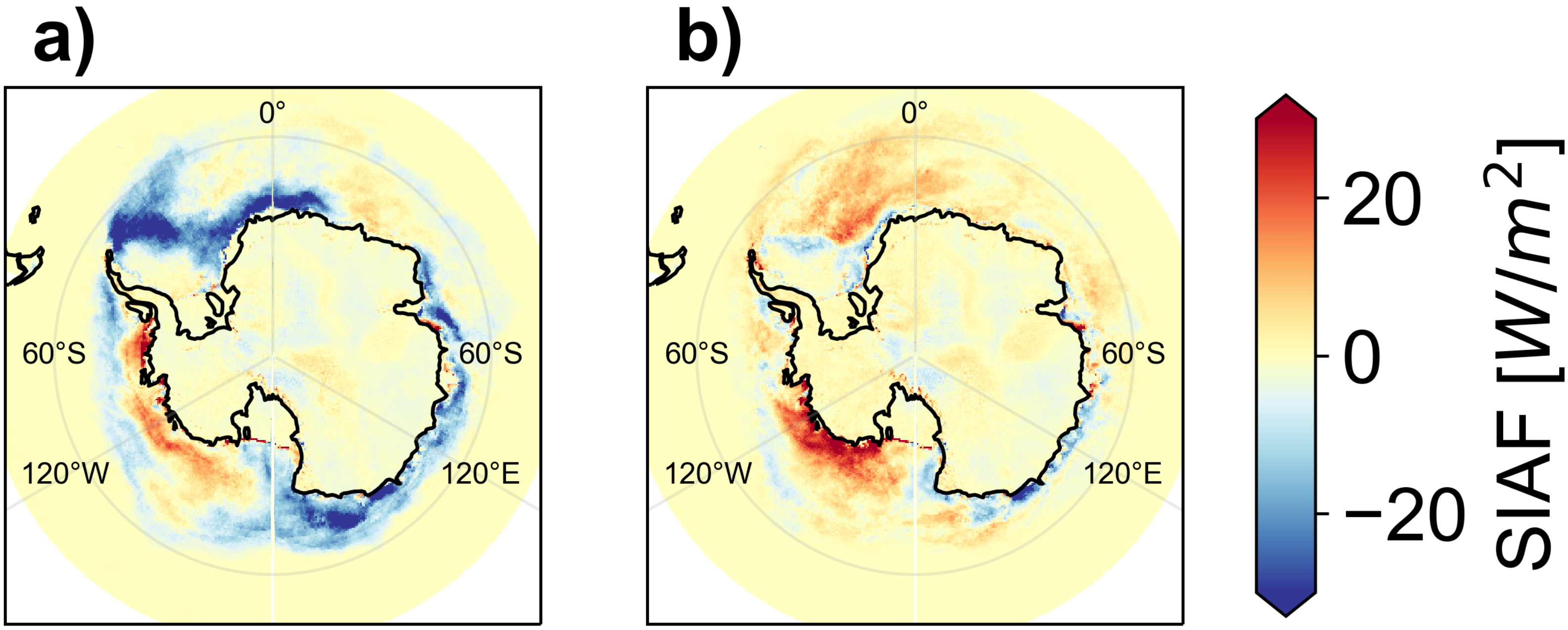
a)
0°
60°S
60°S
120°W
120°E
b)
0°
60°S
60°S
120°W
120°E
20
0
−20
SIAF [W/m^2]

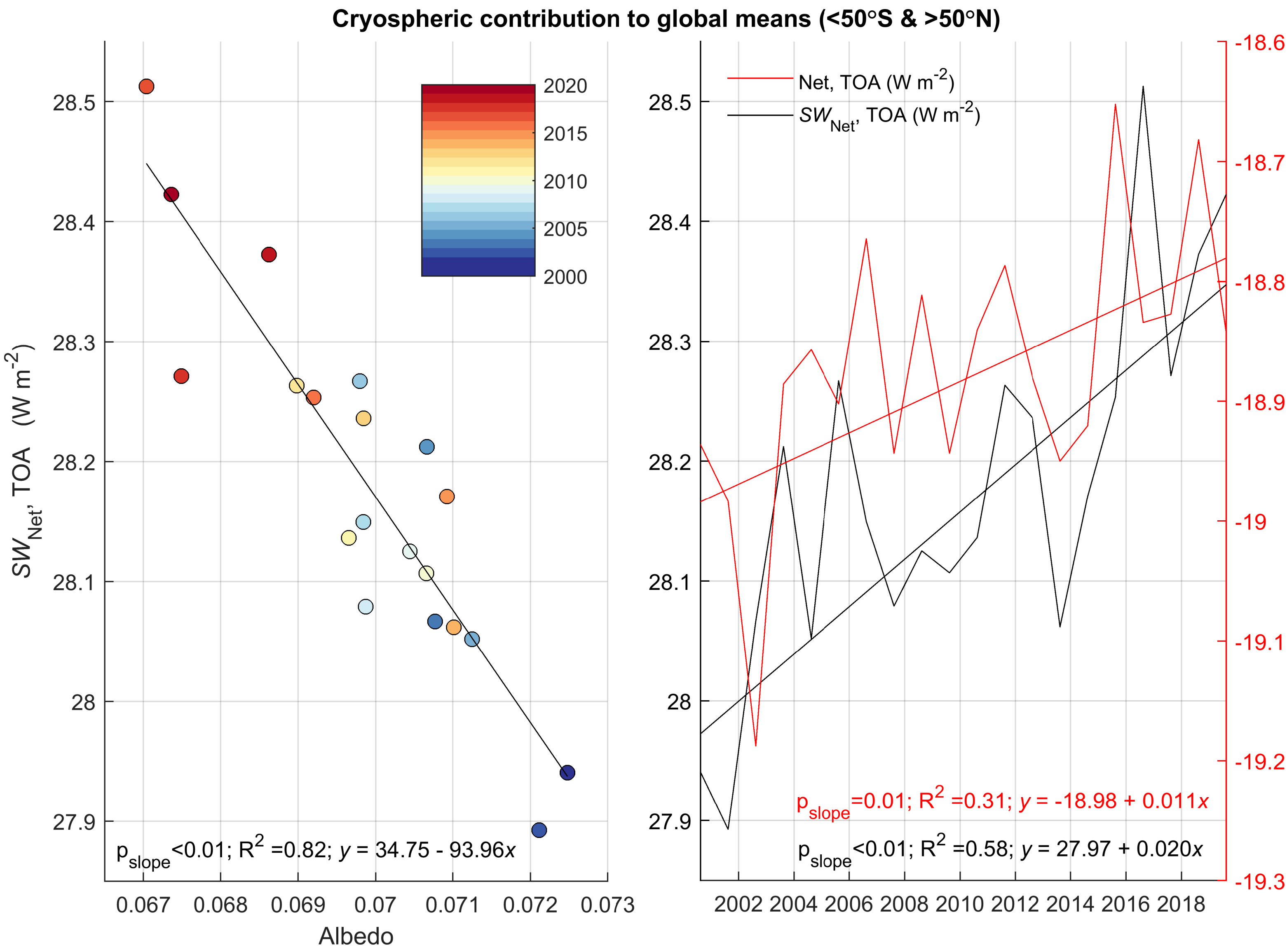
Cryospheric contribution to global means (<50°S & >50°N)
SW_{Net}, TOA (W m^{-2})
Albedo
2020
2015
2010
2005
2000
p_{slope}<0.01; R^2 =0.82; y = 34.75 - 93.96x
Net, TOA (W m^{-2})
SW_{Net}, TOA (W m^{-2})
p_{slope}=0.01; R^2 =0.31; y = -18.98 + 0.011x
p_{slope}<0.01; R^2 =0.58; y = 27.97 + 0.020x